Renormalization of self-consistent approximation schemes at finite temperature. II. Applications to the sunset diagram

Hendrik van Hees and Jörn Knoll
GSI Darmstadt, Planckstraße 1, D-64291 Darmstadt, Germany
(Received 28 November 2001; published 24 April 2002)

The theoretical concepts for the renormalization of self-consistent Dyson resummations, devised in the first paper of this series, are applied to first example cases of ϕ^4 theory. In addition to the tadpole (Hartree) approximation, as a novel part the numerical solutions are presented, which include the sunset self-energy diagram into the self-consistent scheme based on the Φ-derivable approximation or the two-particle irreducible effective action concept.

DOI: 10.1103/PhysRevD.65.105005 PACS number(s): 11.10.Gh, 11.10.Wx

I. INTRODUCTION

In the first paper of this series [1] (paper I), we derived the theoretical concepts for the renormalization of the Dyson-equation-based resummation schemes at finite temperature. It could be shown that such truncated self-consistent approximations can be renormalized with counterterm structures solely defined on the vacuum level of the considered approach, if two conditions are met: (a) the underlying exact theory has to be renormalizable and (b) the approximation scheme has to be based on Baym's Φ-derivable concept [2–4], i.e., on a two-particle irreducible (2PI) effective action principle. Thus the self-consistent self-energies Σ are generated from a truncated set of 2PI closed diagrams (called Φ) of the underlying full theory through

$$\Sigma(p)=2i\frac{\delta\Phi[G]}{\delta G(p)}, \tag{1*}$$

where $\Phi[G]$ is a functional of the self-consistent propagator $G(p)$ in the momentum representation (as in I, an asterisk behind an equation number implies that the corresponding relations are only valid at the regularized level, while all other equations are valid also for the renormalized quantities). To repeat, the main issue is not to render any divergent loops finite; this has been pursued many times. The aim is to deploy the counterterm structure such that it is entirely determined at the vacuum level of the self-consistent scheme. In addition to the explicitly visible divergences, this implies resolving also the nested and overlapping vacuum divergences hidden in the self-consistent matter parts of the propagator.

In I, we have given proof that for the self-energy this can be done for any Φ-derivable approximation, provided the underlying quantum field theory is renormalizable in the usual sense. Thereby, the counterterm structure results from closed equations on the vacuum level, implicitly generating a particular though infinite subset of counterterms. The complexity of the ensuing equation is similar to that for the self-energy.

Thereby, it is of particular importance that the entire counterterm structure is *consistently constructed solely and only within the effective action defined by the chosen approximation to* Φ. This implies that, e.g., the so-obtained counterterm scheme and thus the behavior of the running coupling constant clearly deviate from the true one at orders beyond those included in Φ. If these rules are not watched, one may face uncompensated divergences as recently encountered in the detailed work of Braaten and Petitgirard [5]. They tackled the same problem, however using different techniques in terms of a restricted ansatz for the propagator. Uncompensated singularities arose from the fact that the used β function was not the one pertaining to the self-consistent scheme but taken from the full β function calculated up to the fifth loop order. Furthermore, it is still not clear to us how in their approach the hidden and nested vacuum subdivergences can be resolved such that one arrives at a counterterm structure solely defined on the self-consistent vacuum level ($T=0$). In our case, the latter leads to a renormalized Bethe-Salpeter equation for the vacuum four-point function consistent with the chosen approximation level for the Φ functional.

In I, we also showed that the generating functional $\Gamma[\varphi,G]$ and thus the thermodynamic potential can be rendered finite with counterterms solely defined on the vacuum level of the self-consistent scheme. Again, it is crucial to expand the functional around the *solutions of the corresponding self-consistent approximation for the vacuum*. It is not possible to render arbitrary parts of Γ finite for themselves since it is important to use the stationarity of Γ for the solution of the vacuum equations of motion. In particular, terms linear in the matter parts of the propagator are singular and only drop out if the vacuum part is solved self-consistently.

For self-consistent Dyson resummation schemes, it is well known [6] that they may violate symmetry properties such as crossing symmetry, masslessness of Nambu-Goldstone modes, conservation laws, etc., at a level beyond that of one-point functions, i.e., on the correlator level at orders beyond those included in Φ. We will devote a forthcoming paper [7] in this series to the issue of how to extend the scheme such that symmetry violations are indeed cured.

In this paper, we give first numerical solutions for the leading and the next-to-leading order of the self-consistent Dyson equations for the ϕ^4 theory, which is defined by the Lagrangian

$$\mathcal{L}=\tfrac{1}{2}(\partial_\mu\phi)(\partial^\mu\phi)-\frac{m^2}{2}\phi^2-\frac{\lambda}{4!}\phi^4. \tag{2}$$

In the symmetric phase, $\langle\phi\rangle=0$, the first diagrams contributing to Φ and Σ are

$$i\Phi = \tfrac{1}{2}\,\cdots, \tag{3*}$$

$$-i\Sigma = \;+\cdots, \tag{4*}$$

where all lines represent self-consistent propagators. The leading-order diagram gives rise to the tadpole (Hartree) approximation for the self-energy, which, frequently considered in the literature (see, for instance, [6,8]), leads to the standard gap equation. Here it is given as the most simple example for our general renormalization scheme. The next-to-leading order includes the sunset diagram for the self-energy. While in the tadpole case the self-energy is real and constant, with the sunset term the self-energy becomes momentum-dependent and complex. Thus the particles acquire a finite spectral width due to collisions with the surrounding matter. With the sunset diagram one enters a new stage of sophistication, both as far as the counterterm structure is concerned and with respect to the numerical solution of the resulting self-consistent equations.

The first numerical investigations of the self-energy are presented which result from the two explicitly given diagrams in Eq. (4*). We could improve the numerical accuracy immensely compared to the status given in [9], where we restricted ourselves to the computation of the imaginary parts of the self-energy to avoid problems with renormalization.

The paper is organized as follows. In Sec. II, we briefly summarize the results of I as far as we need the formulas for the numerical calculations. In Sec. III, we solve the tadpole approximation (gap equation) and in Sec. IV the next-to-leading-order approximation including the sunset diagram.

Throughout the paper, we work in the momentum-space representation within the real-time field theory formalism for the self-energies and propagators. Thus, if not stated otherwise, self-energies and Green's functions are contour matrix valued in the sense of the Schwinger-Keldysh real-time contour [10–12]. There vertices belonging to time arguments on the time and antitime ordered branches are labeled by $-$ and $+$ superscripts, respectively. The integration sense is accounted for by assigning the values $\mp i\lambda$ to the bare vertex depending on its placement on the $\{-\}$ or $\{+\}$ branches of the contour.

II. THE RENORMALIZED EQUATIONS OF MOTION

In I, we have shown that arbitrary self-consistent approximations given by the Φ-derivable concept (1*) can be renormalized with counterterms defined on the vacuum level. Thereby, the renormalized self-energy as well as the thermodynamic potential are finite and consistent with one another.

For the renormalization procedure, the self-energy has to be split into three parts, namely the pure vacuum part [which is of divergence degree $\delta(\Sigma^{(\mathrm{vac})})=2$], the part $\Sigma^{(0)}$ with divergence degree $\delta(\Sigma^{(0)})=0$, containing explicit and hidden vacuum subdivergences, and the rest $\Sigma^{(r)}$ with $\delta(\Sigma^{(r)})=-2$, which contains only explicit vacuum subdivergences with corresponding counterterms

$$\Sigma=\Sigma^{(\mathrm{vac})}+\Sigma^{(0)}+\Sigma^{(r)}. \tag{5}$$

The self-consistent Green's function G follows from the Dyson equation in contour matrix form,

$$\Delta^{-1}G=1+\Sigma G. \tag{6}$$

Here Δ is the free Green's function on the contour. In view of Eq. (5), the self-energy within the Green's function needs two subtractions to render its loops finite:

$$\mathrm{i}G=\mathrm{i}G^{(\mathrm{vac})}+\underbrace{\mathrm{i}G^{(\mathrm{vac})}\Sigma^{(0,\mathrm{div})}G^{(\mathrm{vac})}+\mathrm{i}G^{(\mathrm{r})}}_{\mathrm{i}G^{(\mathrm{matter})}}= \;+\;+\;. \tag{7}$$

The subtraction only affects contour diagonal pieces of the propagator, since loops containing mixed contour vertices are finite for themselves. Thus

$$iG^{(\mathrm{vac})}(p)=\begin{pmatrix} iG^{--(\mathrm{vac})}(p) & 0 \\ 0 & iG^{++(\mathrm{vac})}(p)\end{pmatrix},$$
$$i\Sigma^{(0;\mathrm{div})}(p)=\begin{pmatrix} i\Sigma^{--(0)}(p) & 0 \\ 0 & i\Sigma^{++(0)}(p)\end{pmatrix}, \tag{8}$$

and likewise $\Sigma^{(\mathrm{vac})}$ are diagonal. While $G^{(\mathrm{vac})}$ and $\Sigma^{(\mathrm{vac})}$ are given by the (anti)time-ordered self-consistent expressions given by the Φ-derivable scheme on the vacuum level, $\Sigma^{(0)}$ accounts for the self-energy parts linear in $G^{(\mathrm{matter})}$. The three right-hand-side terms of Eq. (7) are of divergence degree -2, -4, and -6, respectively. It is important to notice that only the full self-consistent propagator and self-energy, G and Σ, obey the equilibrium conditions [Kubo-Martin-Schwinger (KMS)] among their four contour components, cf. Eqs. (A14)–(A18) in I. The components of subtracted pieces like $G^{(\mathrm{matter})}$, $\Sigma^{(0)}$, or $\Sigma^{(r)}$ obey no direct equilibrium relations as they result from differences of finite temperature with vacuum terms. Here we see an advantage in the real-time formalism which naturally permits this decomposition into vacuum and matter pieces of all dynamical quantities.

The contour diagonal parts of $\Sigma^{(0)}$ and $\Sigma^{(r)}$ contribute only at finite temperature. Due to Lorentz invariance, the

vacuum self-energy and the Green's function are functions of $s=p^2$. The vacuum self-energy is renormalized according to the rules of the on-shell renormalization scheme, i.e.,

$$\Sigma^{(\mathrm{vac})}(s=m^2)=0, \quad \partial_s\Sigma^{(\mathrm{vac})}(s=m^2)=0, \tag{9}$$

which defines m to be the physical mass of the particles and normalizes the wave functions such that the residuum of the Green's function at $s=m^2$ is equal to 1. As we shall see in the following, the renormalization procedure used to calculate the vacuum parts, and subsequently needed for the temperature-dependent pieces of the self-energy, allows us to choose any renormalization scheme. Especially, it is possible to use ''mass-independent'' minimal subtraction schemes (MS [13] or $\overline{\mathrm{MS}}$ [14] of dimensional regularization) so that the renormalization program shown in I is applicable also for the massless case. For the renormalization of the self-energy and the 2PI-functional $\Gamma[G]$, it is crucial to split all quantities into vacuum ($T=0$) and finite-temperature parts by the procedure given above.

As shown in I, this procedure allows us to define the generating functional in its dependence on the in-matter parts of the propagator with the self-consistent solution given by the stationary point. Simultaneously, this leads to the renormalized thermodynamic potential. All divergences indeed compensate if and only if the vacuum level is solved and renormalized entirely within the same approximation level as used for the finite-temperature parts. This fact together with the *stationarity conditions of the generating functional at* $T=0$ for the vacuum equations of motion avoid the singularity problems encountered in [5].

In $\Sigma^{(0)}$, the in-matter part of the propagator is involved in logarithmically divergent loops which imply hidden divergences. As shown in I, these can be resolved with the following result:

$$\Sigma^{(0)}(p)=\int\frac{d^4l}{(2\pi)^4}\{[\Gamma^{(4)}(l,p)-\Gamma^{(4,\mathrm{vac})}(l,0)]\times G^{(\mathrm{matter})}(l)+\Lambda(0,l)G^{(r)}(l)\}. \tag{10}$$

Here, in consistency with the Dyson equation, the four-point function $\Gamma^{(4)}(p,q)$ is generated also from Φ through

$$\Gamma^{(4)}(p,q)=2\left(\frac{\delta^2\Phi[G]}{\delta G(p)\,\delta G(q)}\right)^{(\mathrm{ren})}_{T\to 0^+}. \tag{11}$$

The counterterm $\Gamma^{(4,\mathrm{vac})}$ contains only the contour diagonal parts (all vertices placed on one side of the real-time contour) of $\Gamma^{(4)}$. This function is 2PI in the channel $p\to q$, i.e., one cannot disconnect the diagrams by cutting two lines and separating the lines carrying the momenta p and q. It contains only vacuum pieces and can straightforwardly be renormalized with $\Gamma^{(4,\mathrm{vac})}(0,0)=\pm\lambda/2$. At the same time, this four-point function defines the kernel for the vacuum s-channel Bethe-Salpeter equation defining the two-particle reducible (2PR) four-point function $\Lambda(p,q)$. In Eq. (10), we only need the half-sided $\Lambda(0,p)$, which, as one of the crucial points of the Bogoliubov-Parasiuk-Hepp-Zimmermann (BPHZ) renormalization procedure [15,16], is given by the finite equation

$$\Lambda(0,p)=\pm\frac{\lambda}{2}+\Gamma^{(4,\mathrm{vac})}(0,p)+i\int\frac{d^4l}{(2\pi)^4}\Lambda(0,l)[G(l)]^2[\Gamma^{(4,\mathrm{vac})}(l,p)-\Gamma^{(4,\mathrm{vac})}(l,0)], \tag{12}$$

again involving only contour diagonal terms. Here we inserted the renormalization condition $\Lambda(0,0)=\pm\lambda/2$.

The expression (10) for $\Sigma^{(0)}$ void of the $\Lambda(0,l)$ part would correspond to a naive subtraction, which indeed is finite, however it implies T-dependent counterterms. As explained in I, only the entire expression (10) guarantees a counterterm structure solely defined on the self-consistent vacuum level.

The perturbative view

The above procedure defines the self-consistent renormalization scheme in terms of the corresponding self-consistent vacuum propagator $G^{(\mathrm{vac})}$, the vacuum four-point function $\Lambda(0,l)$, and the self-consistent in-matter pieces of the propagator $G^{(\mathrm{matter})}$ or $G^{(r)}$. As an illustration, we briefly quote the corresponding perturbative (1PI) view of the scheme, expanding the full self-energy in terms of the vacuum propagator in contour matrix notation satisfying the equilibrium relations KMS at the given temperature T,

$$iG^{(\mathrm{vac},T)}(p)=\begin{pmatrix} iG^{--(\mathrm{vac})}(p) & 0\\ 0 & iG^{++(\mathrm{vac})}(p)\end{pmatrix}+\rho^{(\mathrm{vac})}(|p_0|,\vec{p})\begin{pmatrix} n(p_0) & \Theta(-p_0)+n(p_0)\\ \Theta(p_0)+n(p_0) & n(p_0)\end{pmatrix},$$

$$= \quad \text{———} \quad + \quad \cdots\cdots\cdots \tag{13}$$

with the vacuum spectral function and thermal Bose-Einstein weight defined by

$$\rho^{(\mathrm{vac})}(p)=-2\,\mathrm{Im}\,G_R^{(\mathrm{vac})}(p)=-2\,\mathrm{sgn}(p_0)\mathrm{Im}\,G^{--(\mathrm{vac})},$$

$$n(p_0)=\frac{1}{\exp(\beta|p_0|)-1}. \tag{14}$$

As discussed in I, loops involving the Θ functions or the thermal weights summarized by the dotted line are always finite.

For the self-consistent scheme of tadpole and sunset, the following types of 1PI diagrams are resummed to the full self-consistent self-energy:

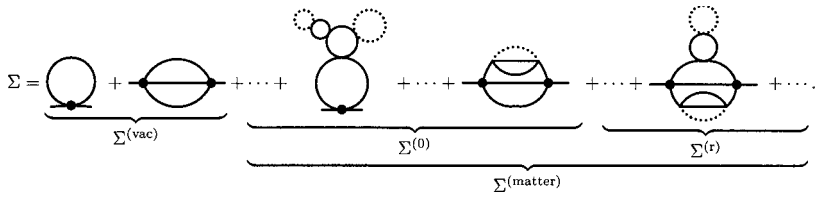

(15*)

Here the diagrams for $\Sigma^{(\mathrm{matter})}$ are generated by iterative insertions of the diagrams of $\Sigma^{(\mathrm{vac})}$, replacing one or more plain lines by dotted ones with the constraint that due to the self-consistency at the vacuum level, *all pure vacuum self-energy insertions are to be excluded*. In $\Sigma^{(\mathrm{matter})}$ vacuum subdiagrams (plain lines) with four external lines are logarithmically divergent and need to be renormalized. Their sum defines the renormalized four-point function Λ. If the latter include the external points (full dots), they contribute to $\Sigma^{(0)}$, defined in Eq. (5). All other terms, like the last term, contribute to $\Sigma^{(r)}$.

III. THE TADPOLE APPROXIMATION

The tadpole approximation is given by

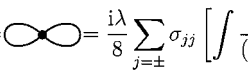

$$\mathrm{i}\Phi[G] = = \frac{\mathrm{i}\lambda}{8}\sum_{j=\pm}\sigma_{jj}\left[\int\frac{\mathrm{d}^d l}{(2\pi)^d}G^{jj}(l)\right]^2 \tag{16*}$$

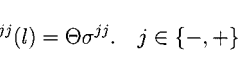

$$-\mathrm{i}\Sigma^{jj} = 2\mathrm{i}\frac{\delta\Phi[G]}{\delta G_{jj}} = = \frac{\lambda}{2}\int\frac{\mathrm{d}^d l}{(2\pi)^d}G^{jj}(l) = \Theta\sigma^{jj}. \quad j\in\{-,+\} \tag{17*}$$

for the unrenormalized Φ functional and self-energy. Here $\sigma=\mathrm{diag}(1,-1)$ accounts for the integration sense on the contour. The self-energy is diagonal in the contour indices. Since the tadpole self-energy is real and constant, the vacuum part vanishes,

$$\Sigma^{(\mathrm{vac})}=0, \tag{18}$$

in view of the physical renormalization condition (9). To find the renormalized equations of motion at finite temperature, we need the renormalized four-point function Λ according to Eq. (10). Because of Eq. (11), we have a constant Bethe-Salpeter kernel,

$$\Gamma^{(4;\mathrm{vac})}=\frac{\lambda}{2} \tag{19}$$

and thus Λ is also constant and determined from its renormalization condition (12),

$$\Lambda^{(\mathrm{vac})}=\frac{\lambda}{2}. \tag{20}$$

In the following, it is sufficient to just consider the $\{--\}$ propagator. Writing $M^2=m^2+\Theta$ from Eq. (6), the self-consistent $\{--\}$ propagator is given by

$$G^{--}(p)=\frac{1}{p^2-M^2+i\eta}-2i\pi n_T(p_0)\,\delta_\eta(p^2-M^2)$$

with

$$\delta_\eta(x)=\frac{1}{\pi}\mathrm{Im}\frac{1}{x-i\eta}=\frac{1}{\pi}\frac{\eta}{x^2+\eta^2}, \tag{21}$$

and the Bose-Einstein function

$$n_T(p_0)=\frac{1}{e^{|p_0|/T}-1}. \tag{22}$$

Since the tadpole self-energy is constant, it is identical with $\Sigma^{(0)}$ and due to Eq. (7) we thus have

$$\begin{aligned}G^{--(r)}(p)&=G^{--}(p)-G^{--(\mathrm{vac})}(p)-\Theta[G^{--(\mathrm{vac})}(p)]^2\\&=\frac{\Theta^2}{(m^2-p^2-i\eta)^2(M^2-p^2-i\eta)}\\&\quad-2\pi i n_T(p_0)\,\delta_\eta(p^2-M^2).\end{aligned} \tag{23}$$

This analytically given result explicitly illustrates that the subtracted part $G^{--(r)}$ of the propagator no longer obeys the finite-temperature KMS and retarded relations [Eqs. (A14)–(A18) in I]. The renormalized effective mass follows from Eqs. (10) and (20) with standard integrals from vacuum-perturbation theory (see, for instance, [17]):

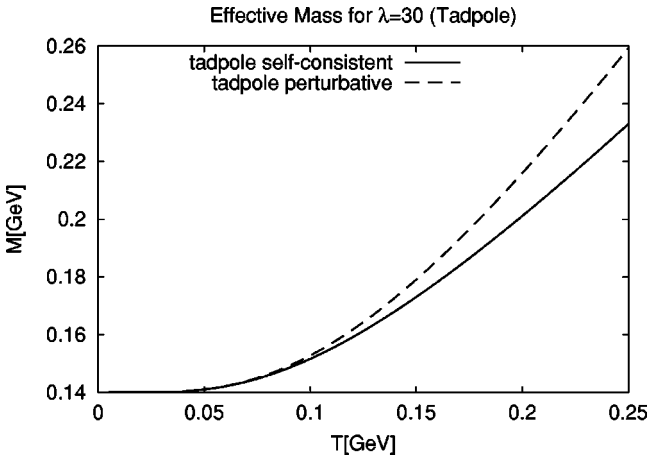

FIG. 1. The solution of the gap equation (24) compared to the naive, i.e., nonresummed one-loop perturbative solution. Both calculations are renormalized in the vacuum in the same way according to the on-shell conditions (9) with $m=0.14\,\mathrm{GeV}$.

$$M^2=m^2+\Theta$$
$$=m^2+\frac{\lambda}{32\pi^2}\left[M^2\ln\left(\frac{M^2}{m^2}\right)-M^2+m^2\right]$$
$$+\frac{\lambda}{4\pi^2}\int_0^\infty dL\,L^2\frac{n_T(\sqrt{L^2+M^2})}{\sqrt{L^2+M^2}}. \tag{24}$$

The solution of this gap equation for $m=0.14\,\mathrm{GeV}$ and $\lambda=30$ is shown in Fig. 1.

The self-consistent treatment reduces the mass gap relative to the perturbative result due to the larger mass M entering the self-consistent loop.

The gap equation (24) becomes singular for $m\to 0$ due to the chosen on-shell renormalization condition (9). For the sake of completeness, we give a brief summary about the treatment of the case of vanishing renormalized vacuum mass in the following.

For $m=0$, the renormalization description has to be changed to a so-called ''mass-independent'' renormalization scheme. This concept is most easily established in the dimensional regularization procedure by the so-called minimal subtraction (MS) or modified minimal subtraction ($\overline{\mathrm{MS}}$) schemes where for all renormalization parts, i.e., in our case of ϕ^4 theory the proper n-point vertex functions with $n\leqslant 4$, only the singular terms in $\epsilon=(4-d)/2$ are canceled.

In the present case of the tadpole approximation where the self-energies are momentum-independent, this can be done analytically. Indeed for $m=0$ we have $\Theta=M^2$ and the divergent part of the diagram reads

$$\Theta_\infty=\frac{i\lambda\mu^{2\epsilon}}{2}\int\frac{d^dl}{(2\pi)^d}\frac{1}{l^2-M^2+i\eta}$$
$$=-\frac{\lambda M^2}{32\pi^2}\left[\frac{1}{\epsilon}+1-\gamma-\ln\left(\frac{M^2}{4\pi\mu^2}\right)+O(\epsilon)\right] \tag{25*}$$

in dimensional regularization. Since now the renormalized vacuum propagator is the free massless propagator, i.e.,

$$G_{\mathrm{vac}}(l)=\frac{1}{l^2+i\eta}, \tag{26}$$

an infrared regulating mass scale μ' has to be introduced in order to calculate both the mass and the four-point vertex,

$$\Theta_{\mathrm{vac}}=\frac{i\lambda\mu^{2\epsilon}}{2}\int\frac{d^dl}{(2\pi)^d}\frac{1}{l^2-\mu'^2+i\eta}$$
$$=-\frac{\lambda\mu'^2}{32\pi^2}\left[\frac{1}{\epsilon}+1-\gamma-\ln\left(\frac{\mu'^2}{4\pi\mu^2}\right)+O(\epsilon)\right], \tag{27*}$$
$$\Gamma^{(4)}_{\mathrm{vac}}(0)=\frac{i\lambda\mu^{2\epsilon}}{2}\int\frac{d^dl}{(2\pi)^d}\frac{1}{(l^2-\mu'^2+i\eta)^2}$$
$$=-\frac{\lambda}{32\pi^2}\left[\frac{1}{\epsilon}-\gamma-\ln\left(\frac{\mu'^2}{4\pi\mu^2}\right)+O(\epsilon)\right]$$

with the $\overline{\mathrm{MS}}$ counterterms,

$$\delta m^2=\lim_{\mu'\to 0}\frac{\lambda\mu'^2}{32\pi^2}\left[\frac{1}{\epsilon}-\gamma\right]=0,$$
$$\delta\lambda=\frac{\lambda}{32\pi^2}\left[\frac{1}{\epsilon}-\gamma\right], \tag{28*}$$

which are IR-finite due to the fact that in dimensional regularization the mass counterterm in the $\overline{MS}$ scheme is proportional to the infrared-regulator mass μ'^2. For $m=0$, the renormalized gap equation finally takes the form

$$M^2=-\frac{\lambda M^2}{32\pi^2}\left[1-\ln\left(\frac{M^2}{4\pi\mu^2}\right)\right]$$
$$+\frac{\lambda}{4\pi^2}\int_0^\infty dL\,L^2\frac{n_T(\sqrt{L^2+M^2})}{\sqrt{L^2+M^2}} \tag{29}$$

implying that perturbatively

$$M^2_{\mathrm{pert}}=\frac{\lambda}{4\pi^2}\int_0^\infty dL\,Ln_T(L)=\frac{\lambda}{24}T^2, \tag{30}$$

which follows from Eq. (29) by letting $M\to 0$ on the right-hand side.

IV. THE SUNSET APPROXIMATION

In this section, we calculate the self-consistent self-energy for the next-to-leading-order approximation of the Φ functional numerically. First we have to solve the renormalized Dyson equation for the vacuum and the Bethe-Salpeter (BS) ladder equation for $\Lambda^{(\mathrm{vac})}$, which is needed as input for the temperature-dependent calculation according to Eq. (10).

The Φ functional is given diagrammatically by

$i\Phi =$ 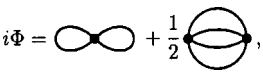 (31*)

while the corresponding self-energy and BS kernel become

$\Sigma =$ 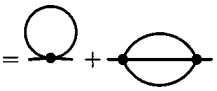 (32*)

$\Gamma^{(4)} =$  . (33*)

For the renormalization parts, it is sufficient to restrict all considerations to one real-time contour branch. For definiteness, we choose the time-ordered branch, i.e., in the following subsections all contour two-point functions denote $\{--\}$ quantities rather than matrices. The physical renormalization scheme (9) implies that the tadpole part of the self-energy is already subtracted such that in the vacuum case we only need to solve for the self-consistent sunset self-energy.

The general strategy will be to combine the BPHZ-renormalization scheme with dimensional regularization and use the spectral representation for the Green's functions (Lehmann representation)

$$G^{(\mathrm{vac})}(p^2)=\int_0^\infty \frac{d(m^2)}{\pi}\,\frac{\mathrm{Im}\,G^{(\mathrm{vac})}(m^2)}{m^2-p^2-i\eta}. \tag{34}$$

All quantities such as the renormalized vacuum self-energy $\Sigma^{(\mathrm{vac})}$, the BS kernel $\Gamma^{(4)}$, and the four-point function Λ are then to be expressed through the vacuum spectral function $\rho=-2\,\mathrm{Im}\,G^{(\mathrm{vac})}$ and corresponding time-ordered kernel functions K_i. The latter express the analytic structure entirely in terms of free-particle properties, however with varying masses. They can then be renormalized by dimensional regularization.

A. The two-propagator loop

A central quantity is the simple loop function contained in Eqs. (32*) and (33*),

$$L^{(\mathrm{reg})}(q^2) = \mathrm{i}$$  $$= \mathrm{i}\int \frac{\mathrm{d}^d l}{(2\pi)^d} G^{(\mathrm{vac})}[(l+q)^2]G^{(\mathrm{vac})}(l^2). \tag{35}$$

This four-point function is logarithmically divergent and to be renormalized with the condition

$$L^{(\mathrm{ren})}(0)=0. \tag{36}$$

With the help of the Lehmann representation (34), it can be expressed as

$$L^{(\mathrm{ren})}(q^2)=\int_0^\infty \frac{dm_1^2}{\pi}\int_0^\infty \frac{dm_2^2}{\pi} K_1^{(\mathrm{ren})}(q^2,m_1^2,m_2^2)\,\mathrm{Im}\,G^{(\mathrm{vac})}(m_1^2)\,\mathrm{Im}\,G^{(\mathrm{vac})}(m_2^2) \tag{37}$$

with the renormalized kernel defined through

$$\begin{aligned} K_1^{(\mathrm{ren})}(q^2,m_1^2,m_2^2)&=K_1^{(\mathrm{reg})}(q^2,m_1^2,m_2^2)-K_1^{(\mathrm{reg})}(0,m_1^2,m_2^2),\\ K_1^{(\mathrm{reg})}(q^2,m_1^2,m_2^2)&=i\int \frac{d^d l}{(2\pi)^d}\,\frac{\mu^{2\epsilon}}{(m_1^2-l^2-i\eta)[m_2^2-(l+p)^2-i\eta]}. \end{aligned} \tag{38}$$

Here the standard notation for dimensionally regularized quantities is used, where $d=4-2\epsilon$ is the space-time dimension and μ denotes the *renormalization scale*.

After a Feynman parametrization, the integral (38) can be expressed in terms of standard formulas of dimensional regularization (see, e.g., [17]), which leads to the result

$$\begin{aligned} K_1^{(\mathrm{reg})}(s,m_1^2,m_2^2)=\frac{1}{16\pi^2 s}\Bigg\{ &-\left(\frac{1}{\epsilon}+2-\gamma\right)s+\lambda(s,m_1,m_2)\left[\mathrm{artanh}\left(\frac{s+m_1^2-m_2^2}{\lambda(s,m_1^2,m_2^2)}\right)+\mathrm{artanh}\left(\frac{s-m_1^2+m_2^2}{\lambda(s,m_1^2,m_2^2)}\right)\right]\\ &+(m_1^2-m_2^2)\ln\left(\frac{m_1}{m_2}\right)+s\,\ln\left(\frac{m_1 m_2}{4\pi\mu^2}\right)\Bigg\} \end{aligned} \tag{39}$$

with the Källén function

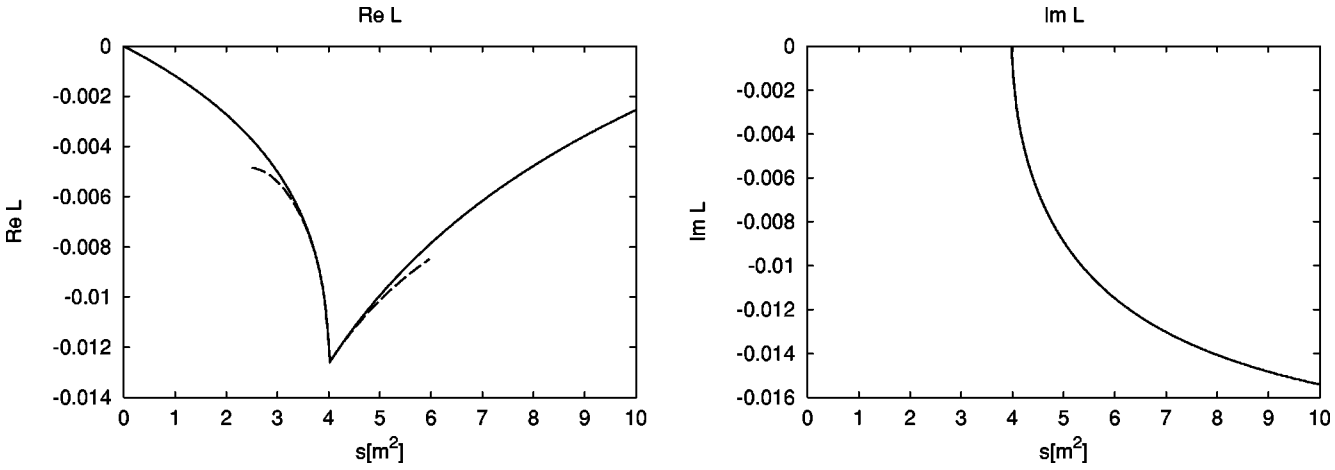

FIG. 2. Real (left) and imaginary part (right) of the loop function L. For the real part, the dashed line shows the approximate behavior (44) around the threshold.

$$\lambda(s,m_1^2,m_2^2)=\sqrt{s^2+m_1^4+m_2^4-2sm_1^2-2sm_2^2-2m_1^2m_2^2}, \tag{40}$$

which is completely symmetric in its three arguments and the branch is determined by the $s+i\eta$ prescription. Here and in the following, we neglect contributions of order $O(\epsilon)$. For the renormalization of this kernel, we also need its value at $s=0$ given by

$$K_1^{(\mathrm{reg})}(0,m_1,m_2)=\frac{1}{16(m_1^2-m_2^2)\pi^2}\left[-\frac{m_1^2-m_2^2}{\epsilon}-1+\gamma+m_1^2\ln\left(\frac{m_1^2}{4\pi\mu^2}\right)-m_2^2\ln\left(\frac{m_2^2}{4\pi\mu^2}\right)\right]. \tag{41}$$

According to Eq. (38), we thus find

$$\begin{aligned}K_1^{(\mathrm{ren})}(s,m_1,m_2)&=[K_1^{(\mathrm{reg})}(s)-K_1^{(\mathrm{reg})}(0)]_{\epsilon\to 0}\\&=\frac{1}{16\pi^2 s}\left\{-s+\frac{(m_1^2-m_2^2)^2-s(m_1^2+m_2^2)}{m_1^2-m_2^2}\ln\left(\frac{m_1}{m_2}\right)\right.\\&\quad\left.+\lambda(s,m_1,m_2)\left[\operatorname{artanh}\left(\frac{s+m_1^2-m_2^2}{\lambda(s,m_1^2,m_2^2)}\right)+\operatorname{artanh}\left(\frac{s-m_1^2+m_2^2}{\lambda(s,m_1^2,m_2^2)}\right)\right]\right\}.\end{aligned} \tag{42}$$

The result for the loop $L(s)$ with $s=q^2$ is given in Fig. 2. The imaginary part is essentially determined by the two-body phase space which opens at $s=4m^2$. To discuss the threshold singularity of L, it is sufficient to study the perturbative result obtained from the pole term of $G^{(\mathrm{vac})}$, which is analytically given as

$$\begin{aligned}L^{(\mathrm{pert})}(s,m^2)&=K_1^{(\mathrm{ren})}(s,m^2,m^2)=\frac{1}{8\pi^2}\left[\sqrt{\frac{s-4m^2}{s}}\operatorname{artanh}\left(\sqrt{\frac{s}{s-4m^2}}\right)-1\right]\\&=\frac{1}{8\pi^2}\left[\sqrt{\frac{s-4m^2}{s}}\left(\ln\frac{\sqrt{s}+\sqrt{s-4m^2}}{2m}-\frac{i\pi}{2}\right)-1\right].\end{aligned} \tag{43}$$

This function is analytic and real for real $s<0$. The analytic continuation to other values of s is given by taking the principal branch of the square root and the artanh functions for $s+i\eta$ with a small $\eta>0$. Close to threshold $s\approx 4m^2$, one obtains the following approximate forms:

$$8\pi^2 L^{(\mathrm{pert})}(s,m^2)=\begin{cases} -\dfrac{\pi}{2}\sqrt{\dfrac{4m^2-s}{s}}-\dfrac{4m^2}{s}+O\left[\left(\dfrac{s-4m^2}{s}\right)^2\right] & \text{for } 0<4m^2-s\ll s, \\ \dfrac{i\pi}{2}\sqrt{\dfrac{s-4m^2}{s}}-\dfrac{4m^2}{s}+O\left[\left(\dfrac{s-4m^2}{s}\right)^2\right] & \text{for } 0<s-4m^2\ll s. \end{cases} \tag{44}$$

Around the threshold, the square-root term causes the singular behavior changing from real to imaginary values, while the remaining log term is entirely real. At large s, the real part of L behaves logarithmically, whereas the imaginary part goes to a constant.

B. The vacuum self-energy

The unrenormalized expression of the two-loop self-energy reads

$$\Sigma^{(\mathrm{vac})}(p^2)=-\frac{\lambda^2}{6}\int\frac{d^dl_1}{(2\pi)^d}\int\frac{d^dl_2}{(2\pi)^d}G^{(\mathrm{vac})}(l_1^2)G^{(\mathrm{vac})}[(l_1+l_2+p)^2]G^{(\mathrm{vac})}(l_2^2). \tag{45*}$$

With the help of Eq. (37), the sunset self-energy with all subdivergences subtracted becomes

$$\overline{\Sigma}^{(\mathrm{vac})}(p)=\frac{i\lambda^2}{6}\int\frac{d^dl_2}{(2\pi)^d}L[(l_2+p)^2]G^{(\mathrm{vac})}(l_2^2). \tag{46}$$

Now we apply the spectral representation for Eq. (35) with one subtraction determined by Eq. (36),

$$L(q^2)=\int_{4m^2}^{\infty}\frac{d(m_3)^2}{\pi}\mathrm{Im}\,L(m_3^2+i\eta)\left(\frac{1}{m_3^2-q^2-i\eta}-\frac{1}{m_3^2-i\eta}\right). \tag{47}$$

Together with the Lehman representation of the propagator (34), this leads to the renormalized vacuum self-energy

$$\Sigma^{(\mathrm{vac})}(s)=\int_{4m^2}\frac{d(m_3^2)}{\pi}\int_{9m^2}\frac{d(m_4^2)}{\pi}K_2^{(\mathrm{ren})}(s,m_3^2,m_4^2)\mathrm{Im}\,L^{(\mathrm{ren})}(m_3^2)\mathrm{Im}\,G^{(\mathrm{vac})}(m_4^2), \tag{48}$$

where due to the renormalization conditions (9) the kernel $K_2^{(\mathrm{ren})}$ is given by

$$K_2^{(\mathrm{ren})}(s,m_3^2,m_4^2)=K_1^{(\mathrm{reg})}(s,m_3^2,m_4^2)-K_1^{(\mathrm{reg})}(m^2,m_3^2,m_4^2)-(s-m^2)[\partial_s K_1^{(\mathrm{reg})}(s,m_3^2,m_4^2)]_{s=m^2}. \tag{49}$$

The cancellation of the contributions from the subtraction of the subdivergences is due to a specialty of the sunset diagram: Here all contracted diagrams are of tadpole structure and therefore independent of the external momentum p and thus are completely canceled by the overall subtractions. The advantage of taking them into account anyway is that at any stage of the calculation we use renormalized functions which can be calculated numerically without using any intermediate regularized functions.

From Eq. (39), we find the analytical expression for the kernel K_2,

$$\begin{aligned} K_2^{(\mathrm{ren})}(s,m_3^2,m_4^2)=&\frac{1}{16\pi^2m^2s}\left\{m^2\lambda(s,m_3,m_4)\times\left[\mathrm{artanh}\left(\frac{s+m_3^2-m_4^2}{\lambda(s,m_3,m_4)}\right)+\mathrm{artanh}\left(\frac{s-m_3^2+m_4^2}{\lambda(s,m_3,m_4)}\right)\right]-s\lambda(m^2,m_3,m_4)\right. \\ &\left.\times\left[\mathrm{artanh}\left(\frac{m^2+m_3^2-m_4^2}{\lambda(m^2,m_3,m_4)}\right)+\mathrm{artanh}\left(\frac{m^2-m_3^2+m_4^2}{\lambda(m^2,m_3,m_4)}\right)\right]\right\}+\frac{(s-m^2)[(m_3^2-m_4^2)^2-m^2(m_3^2+m_4^2)]}{16\pi^2m^4\lambda(m^2,m_3,m_4)} \\ &\times\left[\mathrm{artanh}\left(\frac{m^2+m_3^2-m_4^2}{\lambda(m^2,m_3,m_4)}\right)+\mathrm{artanh}\left(\frac{m^2-m_3^2+m_4^2}{\lambda(m^2,m_3,m_4)}\right)\right]-\frac{s-m^2}{16\pi^2m^2}+\frac{(m_3^2-m_4^2)(s-m^2)^2}{16\pi^2m^4s}\ln\left(\frac{m_3}{m_4}\right). \end{aligned} \tag{50}$$

Equations (37) and (48), supplemented by the Dyson equation

$$G^{(\mathrm{vac})}(p)=\frac{1}{p^2-m^2-\Sigma^{(\mathrm{vac})}(p^2)+i\eta}, \tag{51}$$

form the closed set of renormalized equations of motion, which were solved with the analytically given kernels $K_1^{(\mathrm{ren})}$ and $K_2^{(\mathrm{ren})}$ from Eqs. (42) and (50). For the integrals (37) and (48), a simple adaptive Simpson integrator was used. We have chosen $m=m_\pi=140$ MeV for the mass and $\lambda=30$. As Fig. 3 shows, for this coupling there is no visible difference between the

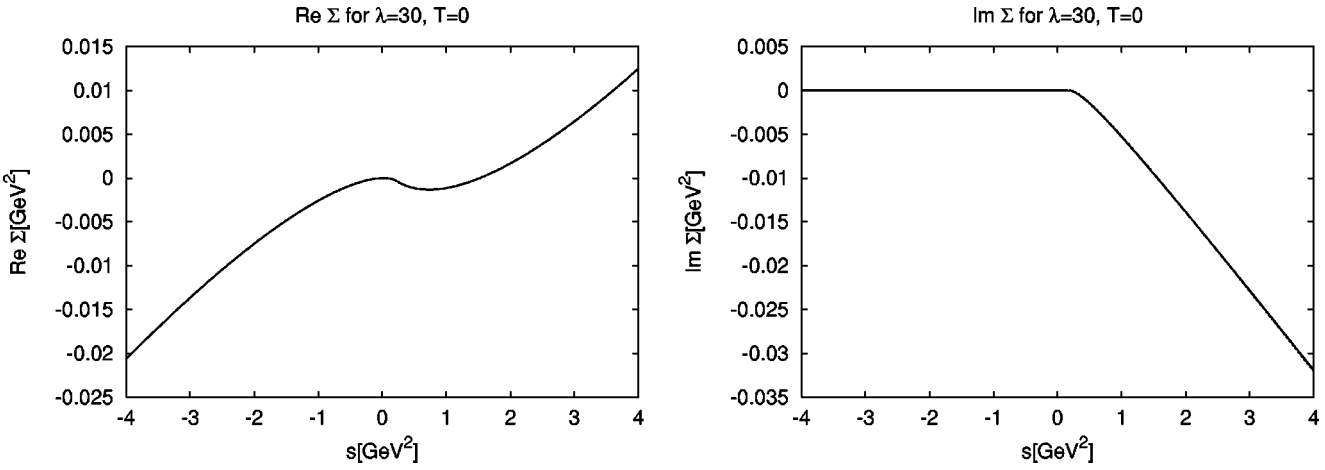

FIG. 3. Real (left) and imaginary part (right) of the sunset self-energy. The perturbative and the self-consistent result lie on top of each other due to the large threshold at $s=9m^2$.

perturbative and the self-consistent result since the main contribution comes from the pole term of the propagator, while the continuous part, which starts at a threshold of $s=9m^2$, is suppressed. Thus, due to our renormalization scheme, where m is the physical mass parameter, the pole-term result essentially coincides with the perturbative one.

C. The Bethe-Salpeter function

The renormalized Bethe-Salpeter kernel $\Gamma^{(4,\mathrm{ren})}$ defined in Eq. (11) reads

$$\Gamma^{(4,\mathrm{ren})}(l,p) := \Gamma^{(4,\mathrm{ren})}[(l-p)^2] = \frac{\lambda}{2} + \lambda^2 L^{(\mathrm{ren})}[(l-p)^2]. \tag{52}$$

Since, as shown above, the pole term essentially determines the loop function L, we simplified the task to solve Eq. (10) by using the free propagator

$$\Delta(p^2) = \frac{1}{p^2 - m^2 + i\eta} \tag{53}$$

instead of the self-consistent vacuum $G^{(\mathrm{vac})}$.

Subtracted dispersion relations for $\Gamma^{(4,\mathrm{ren})}$ and $\Lambda^{(\mathrm{ren})}$ and the renormalization conditions $\Gamma^{(4,\mathrm{ren})}(0,0) = \Lambda^{(\mathrm{ren})}(0,0) = \lambda/2$ provide the renormalized integral equation

$$\Lambda^{(\mathrm{ren})}(0,p^2) = \Gamma^{(4,\mathrm{ren})}(p^2) + i\int \frac{d^4l}{(2\pi)^4}[\Delta(l^2)]^2 \left\{ \int_{4m^2}^{\infty} \frac{d(m_2^2)}{\pi} \mathrm{Im}\,\Gamma^{(4,\mathrm{ren})}(m_2^2) \frac{2lp - p^2}{[m_2^2 - (l-p)^2 - i\eta](m_2^2 - l^2 - i\eta)} \times \left[\int \frac{d(m_1^2)}{\pi m_1^2} \frac{l^2\,\mathrm{Im}\,\Lambda^{(\mathrm{ren})}(0,m_1^2)}{m_1^2 - l^2 - i\eta} + \frac{\lambda}{2} \right] \right\}. \tag{54}$$

Again the l integration can be performed with the help of standard perturbation theory integrals leading to the kernels

$$K_3^{(\mathrm{ren})}(p^2,m_1,m_2) = i\int \frac{d^4l}{(2\pi)^4} \frac{1}{(m^2 - l^2 - i\eta)^2} \frac{l^2(2lp - p^2)}{(m_1^2 - l^2 - i\eta)[m_2^2 - (l-p)^2 - i\eta]},$$
$$K_4^{(\mathrm{ren})}(p^2,m_2) = i\int \frac{d^4l}{(2\pi)^4} \frac{2lp - p^2}{(m^2 - l^2 - i\eta)^2[m_2^2 - (l-p)^2 - i\eta]}, \tag{55}$$

which can be related to the previous kernel K_1 through the identity

$$[\Delta(l^2)]^2 = -\frac{1}{2m}\partial_m \frac{1}{m^2 - l^2 - i\eta}. \tag{56}$$

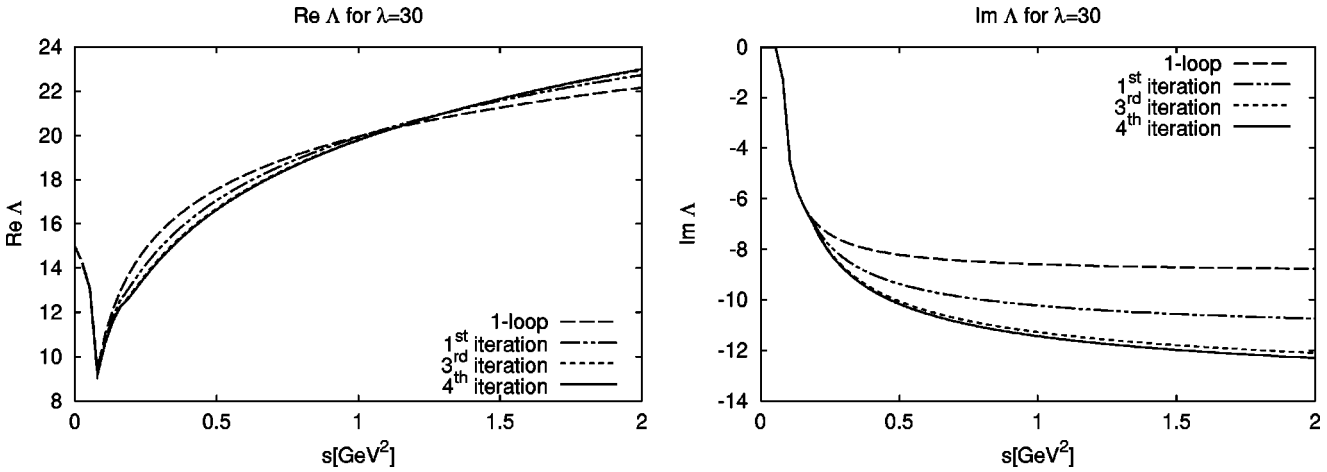

FIG. 4. Real (left) and imaginary part (right) of the Λ function. The plot shows that after three iterations the solution is already stable.

We start with the calculation of K_4 defined in Eq. (55) and write it in the form

$$K_4(s,m,m_2) = -\frac{i}{2m}\partial_m \int \frac{d^4l}{(2\pi)^4}\frac{1}{m^2-l^2-i\eta}\left[\frac{1}{m_2^2-(l-p)^2-i\eta}-\frac{1}{m_2^2-l^2-i\eta}\right], \tag{57}$$

which can be expressed in terms of $K_1^{(\mathrm{ren})}$:

$$K_4(s,m,m_2) = -\frac{1}{2m}\partial_m K_1(s,m,m_2) = -\frac{1}{16\pi^2 s}\left\{\frac{s}{m_2^2-m^2}+\frac{(m^2-m_2^2-s)}{\lambda(s,m,m_2)}\times\left[\operatorname{artanh}\left(\frac{s+m_1^2-m_2^2}{\lambda(s,m_1,m_2)}\right)\right.\right.$$
$$\left.\left.+\operatorname{artanh}\left(\frac{s-m_1^2+m_2^2}{\lambda(s,m_1,m_2)}\right)\right]+\frac{(m^2-m_2^2)^2+2m_2^2 s}{(m^2-m_2^2)^2}\ln\left(\frac{m}{m_2}\right)\right\}. \tag{58}$$

The integrand of K_3, cf. Eq. (55), can be rewritten as follows:

$$\frac{i}{m^2-l^2-i\eta}\frac{l^2}{m_1^2(m_1^2-l^2-i\eta)}\frac{p^2-2lp}{(m_2^2-l^2-i\eta)[m_2^2-(l-p)^2-i\eta]} = -\frac{i}{2m}\partial_m\frac{1}{m_1^2-m^2}\left(\frac{1}{m^2-l^2-i\eta}-\frac{1}{m_1^2-l^2-i\eta}\right)$$
$$-\frac{1}{m_1^2(m^2-l^2-i\eta)}\left[\frac{1}{m_2^2-(l-p)^2-i\eta}-\frac{1}{m_2^2-l^2-i\eta}\right]. \tag{59}$$

The integration of Eq. (59) then leads to

$$K_3(s,m,m_1,m_2) = \frac{K_1(s,m_1,m_2)-K_1(s,m,m_2)}{(m^2-m_1^2)^2}+\frac{m^2-2m_1^2}{(m^2-m_1^2)m_1^2}K_4(s,m,m_2). \tag{60}$$

With the so-defined kernels, we can express Eq. (54) as follows:

$$\Lambda^{(\mathrm{ren})}(0,p^2) = \Gamma(p^2)+\int_{4m^2}^{\infty}\frac{dm_1^2}{\pi m_1^2}\frac{dm_2^2}{\pi}K_3(p^2,m_1,m_2)\,\mathrm{Im}\,\Lambda^{(\mathrm{ren})}(0,m_1^2)\,\mathrm{Im}\,\Gamma^{(4,\mathrm{ren})}(m_2^2)$$
$$+\frac{\lambda}{2}\int_{4m^2}^{\infty}\frac{dm_2^2}{\pi}K_4(p^2,m_2)\,\mathrm{Im}\,\Gamma^{(4,\mathrm{ren})}(m_2^2). \tag{61}$$

Figure 4 shows the solution of this renormalized equation of motion in comparison with the one-loop approximation $\Gamma^{(4,\mathrm{ren})}$. As the figure shows, the solution is stable after three iterations.

D. The temperature-dependent parts

To calculate the temperature-dependent part of the self-energy, we use the analytical properties of the two-point functions and the fact that the retarded propagator fulfills the simple Dyson equation

$$G_R(p)=\frac{1}{p^2-m^2-\Sigma_R(p)}, \tag{62}$$

where the retarded self-energy can be obtained from the $\{--\}$-matrix element via the equilibrium expression

$$\Sigma_R(p)=\mathrm{Re}\,\Sigma^{--}(p)+i\tanh\left(\frac{p_0}{2T}\right)\mathrm{Im}\,\Sigma^{--}(p). \tag{63}$$

As explained in I, both $G^{(\mathrm{vac})}$ and $\Sigma^{(0)}$ are diagonal matrices while the corresponding off-diagonal parts are contained in $G^{(r)}$, because they are of a lower degree of divergence due to explicit $\Theta+n$ factors.

Due to its topology, the sunset diagram has no further vertices besides its two external points. Therefore, the 2PI vacuum four-point function $\Gamma^{(4,\mathrm{vac})}$ is effectively only a two-point function and thus we need only the $\{--\}$ components of the various Green's functions in order to calculate Σ^{--}. This implies

$$G^{--(\mathrm{matter})}=G^{--}-G^{--(\mathrm{vac})},\quad G^{--(r)}=G^{--(\mathrm{matter})}-[G^{--(\mathrm{vac})}]^2\Sigma^{--(0)}. \tag{64}$$

With the help of the renormalized vacuum parts, we obtain for the self-energy

$$\begin{aligned}\Sigma^{--}(p)=\Sigma^{--(\mathrm{vac})}(p)&+i\int\frac{d^4l}{(2\pi)^4}\{\Gamma^{(4,\mathrm{vac})}[(l+p)^2]-\Gamma^{(4,\mathrm{vac})}(l^2)\}G^{--(\mathrm{matter})}(l)+i\int\frac{d^4l}{(2\pi)^4}\Lambda^{(\mathrm{ren})}(0,l^2)G^{--(r)}(l)\\&-\frac{\lambda^2}{2}\int\frac{d^4l_1}{(2\pi)^4}\int\frac{d^4l_2}{(2\pi)^4}G^{--(\mathrm{matter})}(l_1)G^{--(\mathrm{matter})}(l_1+l_2)G^{--(\mathrm{vac})}(l_2+p)\\&-\frac{\lambda^2}{6}\int\frac{d^4l_1}{(2\pi)^4}\int\frac{d^4l_2}{(2\pi)^4}G^{--(\mathrm{matter})}(l_1)G^{--(\mathrm{matter})}(l_1+l_2)G^{--(\mathrm{matter})}(l_2+p).\end{aligned} \tag{65}$$

Note that all vacuum quantities entering here are to be taken in their *renormalized* version and that the remaining integrals are all finite due to power counting.

E. Results

The above finite integrals are to be evaluated numerically. While due to Lorentz invariance the vacuum loops involve just two-dimensional integrations which can numerically be integrated by standard methods, for the in-matter loops only rotational symmetry in three-momentum space can be exploited. For each loop diagram, this leads to three-dimensional integrals for each external momentum $p_0,|\vec{p}|$. We solve these integrals on an equally distant $N\times N$ lattice in these coordinates. Naively, the computing effort would then scale like N^5. However, we succeeded to develop an improved algorithm for the loop integrations, where the computing time scales with N^4 (essentially a gain of more than two orders of magnitude). The lattice implies an infrared cutoff which requires particular care for the treatment of the sharp structures of the vacuum propagator around its on-shell pole. The method at hand was to tabulate the lattice cell integrated values of the propagator and its moment in p_0 given by the analytic result from a linear interpolation in p_0^2 of the inverse propagator at fixed $|\vec{p}|$. The remaining self-energy factors of the integrands are approximated to linear order in p_0^2. The interpolation procedure is adapted to the fact that due to the quadratic pole of the $(G^{--(\mathrm{vac})})^2$ term, one is sensitive to the p_0 derivative (residue) of the remaining integrand. Both the infrared and the UV cutoffs of the lattice have been controlled by varying the lattice spacing and the overall size of the lattice. The final results were achieved with $\Delta p_0=\Delta|\vec{p}|=6.67$ MeV with $N=300$, i.e., a UV cutoff at 2 GeV.

Perturbative results are obtained through Eq. (65) approximating $G^{(\mathrm{matter})}$ by the KMS-temperature part of the free propagator $G^{(\mathrm{vac};T)}$ [last term in Eq. (13); note that here $G^{(r)}=G^{(\mathrm{matter})}$ since $\Sigma^{(\mathrm{vac})}=0$]. The self-consistent solutions are then obtained iteratively through the set of Eqs. (62)–(65). The results for both the perturbative and the self-consistent case are shown in Fig. 5 in a three-dimensional plot over the $(p_0,|\vec{p}|)$ plane, illustrating that all the calculations are performed with the full dependence on energy and momentum. Details can be extracted from the cuts shown for a set of selected momenta in Fig. 6.

The main qualitative results are similar for both the perturbative and the self-consistent calculation: In the vacuum and self-consistent pure tadpole case, the self-energy shows a threshold cut resulting from the decay into three particles, i.e., $p_0^2-\vec{p}^2\geqslant 9M^2$. Adding the sunset self-energy leads to a spectral width which dissolved this threshold such that the self-energy shows spectral strength (imaginary parts) at all energies. While the growing high-energy tail is related to the decay of virtual bosons into three particles, at finite temperature, as a new component, a low-energy plateau in $\mathrm{Im}\,\Sigma^R$ emerges from in-medium scattering processes.

Various balancing effects are encountered for the self-consistent case: For sufficiently large couplings and/or tem-

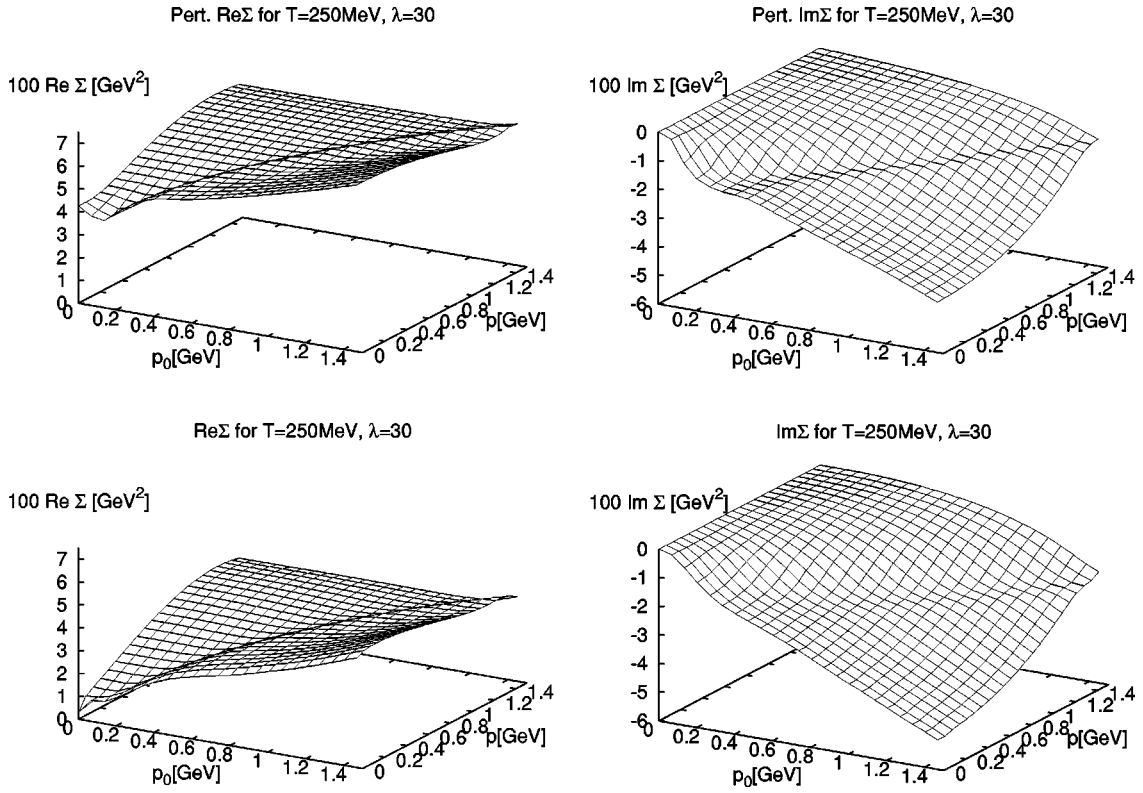

FIG. 5. Real (left) and imaginary part (right) of the perturbative (top) and the self-consistent self-energy for $\lambda = 30$, $m = 140$ MeV, and $T = 250$ MeV. Note that the self-energies are multiplied with a factor 100 in these plots.

peratures, the self-consistent treatment shows quantitative effects on the width. The finite spectral width itself leads to a further broadening of the width and a smoothing of the structures as a function of energy.

This is, however, counterbalanced by the behavior of the real part of the self-energy, which, as discussed below, essentially shifts the in-medium mass upwards. This reduces the available phase space for real processes. With increasing coupling strength λ, a nearly linear behavior of $\mathrm{Im}\,\Sigma^R$ with p_0 results, implying a nearly constant damping width given by $-\mathrm{Im}\,\Sigma^R/p_0$.

The overall normalization of the real part of Σ^R is determined by the renormalization procedure. In this case, there are three counterbalancing effects. First the tadpole loop shifts the mass to higher values. As the tadpole is less effective for higher masses, this effect weakens itself in the self-consistent tadpole treatment, cf., Figs. 1 or 7. However, since the sunset part adds spectral width, it contributes indirectly to the tadpole loop. Since spectral strength at the lower mass side carries higher statistical weights, the tadpole loop in turn leads to a further increase of the mass shift, cf. the perturbative calculations of sunset and tadpole in Fig. 7.

The direct contributions of the sunset terms to the real part of the self-energy become relevant at higher couplings and temperatures. Then the self-consistency leads to significant effects which contribute to a net downshift of the real part of the self-energy or in-medium mass M. The latter effect finally overrules the tadpole shift and indeed leads to an overall negative mass shift compared to the (tadpole-dominated) perturbative result. These effects are illustrated in Fig. 7, where the in-medium effective mass M and width Γ of the corresponding ''quasiparticles'' are plotted against the temperature. Thereby, M and Γ are defined as the quasiparticle energy $M = p_0$ at the vanishing real part of the dispersion relation $[p_0^2 - m^2 - \mathrm{Re}\,\Sigma(p_0,\vec{p})]_{p=(M,\vec{0})} = 0$ for $\vec{p} = 0$ and through $\Gamma = -\mathrm{Im}\,\Sigma(p)/p_0|_{p=(M,\vec{0})}$, respectively.

V. CONCLUSIONS AND OUTLOOK

We have shown that it is possible to use the renormalization scheme, proposed in [1], for numerical investigations of the self-consistent approximations for the self-energy derived from the truncated effective action formalism on the 2PI level. Thereby, it is very important to isolate the divergent vacuum parts consistently, in particular the implicit or hidden ones, from all convergent and, in particular, temperature- or more generally matter-dependent parts. This could be provided by the ansatz given in I for both the propagator and the self-energy. The renormalized vacuum pieces are obtained using the Lehmann representation for all two-point quantities. The resulting integration kernels can then be renormalized by standard techniques. The procedure rests solely on Weinberg's power-counting theorem, i.e., on an analysis of the asymptotic behavior of the propagators.

In this way, both the renormalized vacuum self-energy and four-point functions can directly be obtained from finite equations. For the finite-temperature parts, it is important that they have to be completely excluded from the counterterm structures. This is achieved by the technique developed in I. Exploratory calculations are shown for the symmetric

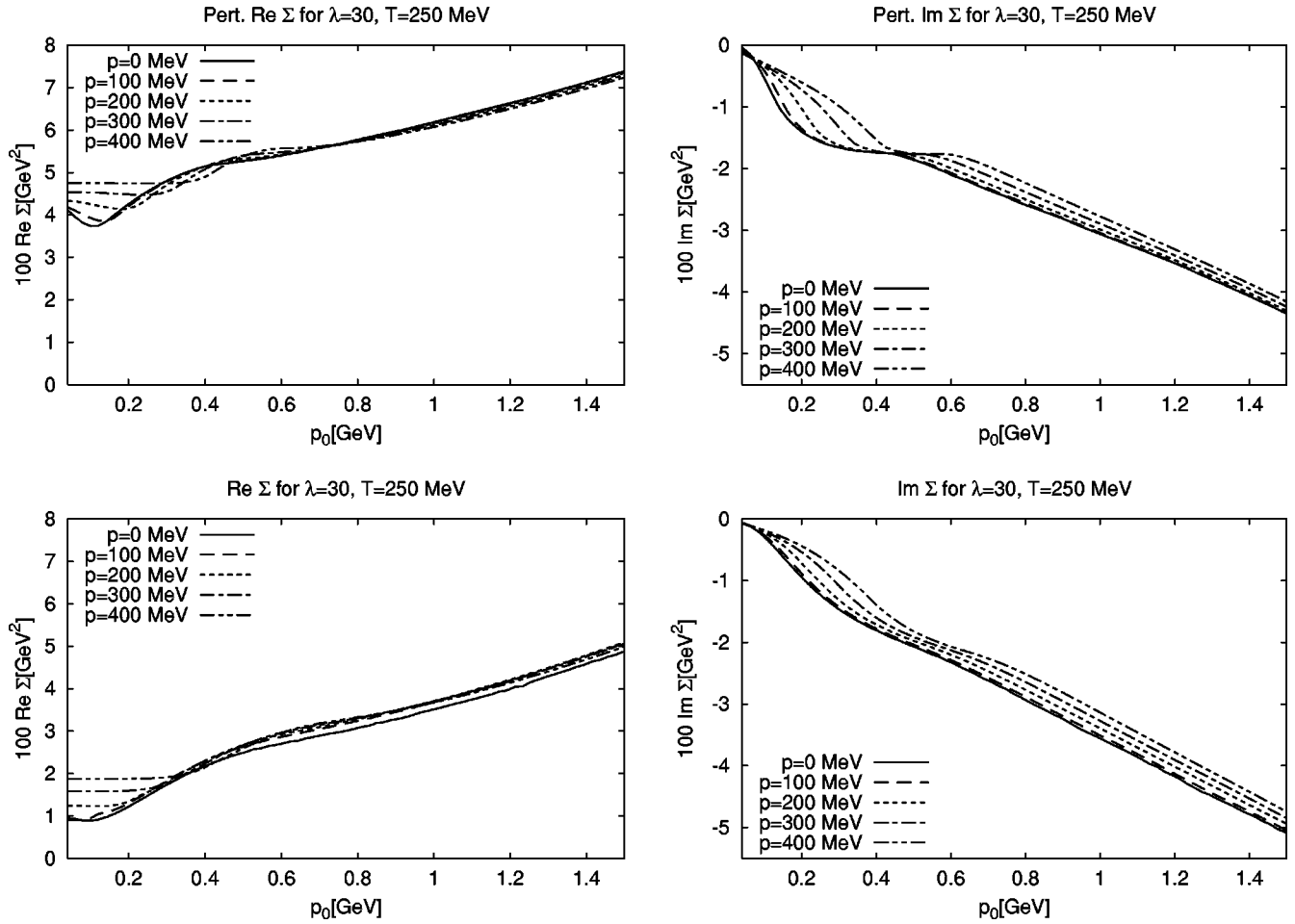

FIG. 6. Real (left) and imaginary part (right) of the perturbative (top) and the self-consistent self-energy for $\lambda = 30$, $m = 140$ MeV, and $T = 250$ MeV as a function of p_0 for various 3-momenta. Note that the self-energies are multiplied by a factor of 100 in these plots.

Wigner-Weyl phase of the $\lambda\phi^4$ model for the self-consistent treatment of both the tadpole and the sunset diagram at finite temperature.

The results promise that the method, which is conserving [2,12] and thermodynamically consistent, can also be applied for the genuine nonequilibrium case, i.e., in quantum transport [18] or for the solution of the renormalized Kadanoff-Baym equations. Numerical studies for nonequilibrium cases (Gaussian initial conditions and spatially homogeneous systems) were already performed in [19–21]. These investigations were undertaken in $1+1$ dimensions. Our renormalization scheme should also be applicable for the nonequilibrium

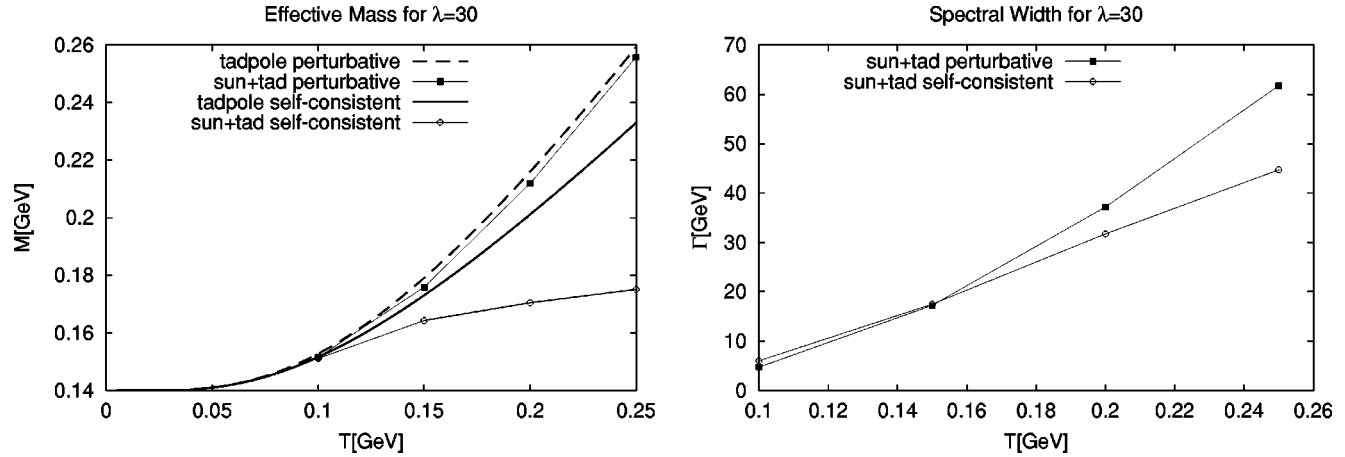

FIG. 7. The in-medium effective masses M (left) and spectral widths Γ (right) of the particles for the various approximations described in the text as a function of the system's temperature T.

case in $1+3$ dimensions and implementable in numerical codes.

The investigation of the symmetry properties of Φ-derivable approximations is the subject of a forthcoming publication [7]. It is known that in general the symmetries of the classical action which lead to Ward-Takahashi identities for the proper vertex functions are violated for the self-consistent Dyson resummation for the functions beyond the one-point level, i.e., on the correlator level. The reason is that, although the *functional* Γ can be expanded with respect to expansion parameters like the coupling or $\hbar$ (loop expansion) or large-N expansions for $O(N)$-type models, the solution of the self-consistent equations of motion contains partial contributions to any order of the expansion parameter. This resummation is of course incomplete and violates even crossing symmetry for the vertices involved in the renormalization procedure. This causes problems concerning the Nambu-Goldstone modes [6] in the broken symmetry case or concerning local symmetries (gauge symmetries) [9] on a level where the gauge fields are treated beyond the classical field level, i.e., on the propagator level.

It can be shown, though, that on top of any solution of a Φ-derivable approximation which is constructed from a symmetric Lagrangian, there exists a nonperturbative effective action $\Gamma_{\rm eff}[\varphi]$ which generates proper vertex functions in the same sense as the 1PI effective action. These *external vertex functions* fulfill the Ward-Takahashi identities of the underlying symmetry. However, in general they coincide with the self-consistent ones only up to one-point order. This fact especially ensures that the expectation values of Noether currents are conserved for the Φ-derivable approximations. Thus usually the so-generated external self-energy and higher vertex functions are different from the Φ-derivable expressions. Details on these considerations will be given in a forthcoming paper [7].

ACKNOWLEDGMENTS

We are grateful to J. Berges, J. P. Blaizot, G. E. Brown, P. Danielewicz, B. Friman, Yu. Ivanov, M. Lutz, M. A. Nowak, and D. Voskresensky for fruitful discussions and suggestions at various stages of this work.

[1] H. van Hees and J. Knoll, Phys. Rev. D **65**, 025010 (2002).
[2] G. Baym, Phys. Rev. **127**, 1391 (1962).
[3] J. Luttinger and J. Ward, Phys. Rev. **118**, 1417 (1960).
[4] M. Cornwall, R. Jackiw, and E. Tomboulis, Phys. Rev. D **10**, 2428 (1974).
[5] E. Braaten and E. Petitgirard, Phys. Rev. D (to be published), hep-ph/0107118.
[6] G. Baym and G. Grinstein, Phys. Rev. D **15**, 2897 (1977).
[7] H. van Hees and J. Knoll, Phys. Rev. D (to be published), hep-ph/0111193.
[8] A. Peshier, Phys. Rev. D **63**, 105004 (2001).
[9] H. van Hees and J. Knoll, Nucl. Phys. **A683**, 369 (2001).
[10] J. Schwinger, J. Math. Phys. **2**, 407 (1961).
[11] L. Keldysh, Zh. Eksp. Teor. Fiz. **47**, 1515 (1964) [Sov. Phys. JETP **20**, 1018 (1965)].
[12] Y. B. Ivanov, J. Knoll, and D. N. Voskresensky, Nucl. Phys. **A657**, 413 (1999).
[13] G. 't Hooft, Nucl. Phys. **B61**, 455 (1973).
[14] W. A. Bardeen, A. J. Buras, D. W. Duke, and T. Muta, Phys. Rev. D **18**, 3998 (1978).
[15] N. N. Bogoliubov and O. S. Parasiuk, Acta Math. **97**, 227 (1957).
[16] W. Zimmermann, Commun. Math. Phys. **15**, 208 (1969).
[17] P. Ramond, *Field Theory: A Modern Primer*, 2nd ed. (Addison-Wesley, Redwood City, CA, 1989).
[18] Y. B. Ivanov, J. Knoll, and D. N. Voskresensky, Nucl. Phys. **A672**, 313 (2000).
[19] J. Berges, Nucl. Phys. **A699**, 847 (2002).
[20] J. Berges and J. Cox, Phys. Lett. B **17**, 369 (2001).
[21] G. Aarts and J. Berges, Phys. Rev. D **64**, 105010 (2001).